

# Enhancement the photosensitivity of PPy-NFs/Nanoferrite for Photodetector

Omar A. Hussein<sup>1\*</sup>, T. H. Mubarak<sup>2</sup>, Isam M. Ibrahim<sup>3</sup>

<sup>1</sup>physics, Science, Diyala, Diyala, Iraq, <sup>2</sup>physics, Science, Diyala, Diyala, Ira, <sup>3</sup>physics, Science, Baghdad, Baghdad, Iraq

## Abstract

Polypyrrole nanofibers (PPy-NFs) are sample of conductive polymer. It was synthesized by chemical oxidative polymerization technique. As well as, Nanoparticles of  $Zn_{0.8}Mn_{0.2}Fe_2O_4$  were synthesized by the co-precipitation technique and pursued through treating it with heat in hydrothermal autoclave reactors. The nanocomposite that we obtained by decorating of polypyrrole nanofibers (PPy-NFs) with volume ratios of  $Zn_{0.8}Mn_{0.2}Fe_2O_4$  nanoparticle (50%). The XRD spectra indicated polypyrrole nanofibers (PPy-NFs) is amorphous in nature and the average crystallite size of  $Zn_{0.8}Mn_{0.2}Fe_2O_4$  was (8.54nm). FE-SEM studies revealed that PPy has a nanofibers structure with various diameters. The synthesis method yielded sphere nanoparticles with a modest shift in particle size distribution, according to FESEM pictures. Moreover, the obtained Data analysis from the ultra-violet visible (UV-Vis) spectroscopy showed that PPy-NFs,  $Zn_{0.8}Mn_{0.2}Fe_2O_4$  and PPy-NFs/  $Zn_{0.8}Mn_{0.2}Fe_2O_4$  have band gaps of about (3.9eV, 3.8eV and 4.95eV) respectively. The sensitivity of the photodetector had improved. Where the higher sensitivity of the pure PPy-NFs and  $Zn_{0.8}Mn_{0.2}Fe_2O_4$  were (43.42%) and (81.47%) respectively, at an illumination power of 30 mW for laser diode 405 nm. While the sensitivity was around (103.74%) when PPy-NFs was decorated with ( $Zn_{0.8}Mn_{0.2}Fe_2O_4$ ).

**Keywords:** Polypyrrole nanofibers, Conducting polymer, cation distributions, photodetector Sensitivity.

## 1-Introduction

Materials composed of ferrite and Conductive polymers (CPs) materials can give new or reinforced properties for various purposes and novel applications. "Magneto-polymeric materials" are known for these materials. Conductive polymer-ferrite composites with a regulated constitution create a new practical hybrid between inorganic and organic materials(Nalwa, 2003). The magneto polymeric materials properties which are one of the nanocomposites are extremely affected by the shape, specific surface areas, size scales of its component phases and the degree of phases mixing(S.-J. Ding et al., 2006; Niu, Yang, Hu, Lu, & Han, 2003). These characterizations are very essential for determining structural properties, magnetic behavior(Lu et al., 2005), optoelectronics, optical properties(Caruso, 2001), electrical conductivity(Feng, Mao, Yang, Hou, & Zhu, 2006), microwave absorptions, catalytic effects(Velusamy, Ahamed, & Punniyamurthy, 2004), capacity for drug delivery and controllable release(Xiao & Li, 2008). Various nanocomposites make of polypyrrole and nanoferrite have been lately fabricated(H. Ding, Liu, Wan, & Fu, 2008; Zhong-ai et al., 2006), each of these compounds exhibited very attractive properties. Especially, the polymer that used in this work is nanofibers polypyrrole (NFs-PPy).

One of the magnetic oxides is spinel ferrite. Its regular formula  $MFe_2O_4$  (M=Zn, Co, Mn, Ni, etcin which  $M^{2+}$  and  $Fe^{3+}$  ions could be settling either in octahedral (B) and tetrahedral (A) interstitial sites(O'Hendley, 1999). Structural properties and Chemical of spinel ferrite nanocrystals are affected by their structure, preparation techniques and cation distributions. Therefore, it is important to find new methods to control on the morphology and structure of spinel ferrites(Reddy, Zhou, Huang, & Reddy, 2014). The ferrite that used in this study is  $Zn_xMn_{1-x}Fe_2O_4$  ( $x=0.8$ ) which is a spinel ferrite. Polypyrrole nanofibers (PPy-NFs) can be dispersed with nanoferrites. The magneto-polymer materials with an organized composition can be depended in numerous special objectives due to its important purposes that extend from basic research to different uses and their possessed flowing applications properties(Jiang, Li, & Xu, 2006; Li, Jiang, & Xu, 2006).

The aim of the present work is to synthesize PPy-NFs,  $Zn_{0.8}Mn_{0.2}Fe_2O_4$  and PPy-NFs/ $Zn_{0.8}Mn_{0.2}Fe_2O_4$  in order to study their composition and optical properties. Also, we demonstrate that the photosensitivity of PPy-NFs based photodetectors can be modified by decorating PPy nanofiber with ferrite nanoparticles. This information is very requisite in describing the stability and the suitability of these materials as well as their multi-functions in a variety of applications.

## 2- Experimental work

### 2-1 Synthesis of PPy nanofibers (PPy-NFs)

By chemical polymerization method, 2.5 mM (0.08185 g) methyl orange (MO) (LTD Rubilabor Chemical Co. Spain) was dissolved in de-ionized water (288 ml) and mixed with (14 mM) pyrrole monomer (Sigma Aldrich, China) to form a (Pyrrole monomer- methyl orange) solution that was refrigerated to 3°C by ice bath. The mixture was stirred well until completely dissolved and agglomerates disappeared for 10 minutes. 1.702 (10mM) ( $FeCl_3$ ) (ALPHA chemica) is dissolved in (33 ml) de-ionized water. This is followed by adding a drop-wise during 2 hours into (Py-MO) solution. Thus, these solutions of reaction were stirred for one day (24 hour) in ice baths. The precipitated of PPy-NFs had isolated by filtration and rinsing by acetone,

alcohol and water 3 times each stage to isolate the remaining impurities in PPy-NFs. Lastly, the substance was dried by oven at 75 °C for six hours.

## 2-2 Synthesis of Zn<sub>0.8</sub>Mn<sub>0.2</sub>Fe<sub>2</sub>O<sub>4</sub> nanoparticles

Synthesis of ferrite nanoparticles (Zn<sub>0.8</sub>Mn<sub>0.2</sub>Fe<sub>2</sub>O<sub>4</sub>) was performed by the co-precipitation technology, combined with the hydrothermal synthesis. This method is summarized as the following steps; we dissolve a stoichiometric amounts of FeCl<sub>3</sub> (8.1105g, 50 mM), MnCl<sub>2</sub>.4H<sub>2</sub>O (0.9895g, 5 mM) (ALPHA chemical) and ZnCl<sub>2</sub> (2.7257g, 20 mM) (ROMIL pure chemistry) in deionized water in independent beakers. After that, all moved to a different heat-resistant beaker and continuously stirred for obtaining a homogeneous solution. In addition, in 100ml deionized water, sodium hydroxide (NaOH, 1.25 M L<sup>-1</sup>) (ROMIL pure chemistry) was dissolved separately. Then it was dropped into the metal salt solutions at 27°C until the pH reached 12, ensuring that all of the metal ions in the solution precipitated. After that, the solution had heated at 90°C for 60 minutes and continuously stirred and then switches off and left to cool at 27 °C. The magnetic decantation process was used to separate and collect ferrite nanoparticles. Then, it had washed with deionized water for several times by using a multi-funnels system. In NaOH solution (pH of 12), we stir the mixture to re-disperse the wet product has re-dispersed for 60 minutes. The heat treatment, which was done using the hydrothermal method, was the following step in the fabrication process. The colloidal solution moved to a 250 ml Teflon-lined autoclave reactor. After closing the autoclave tightly, it was put in a furnace at 250°C for 5 hours. Then, it was cooled outdoor naturally at 27 °C. Then, the colloidal solution is filtered followed by washing it with ethanol and deionized water several times so the PH becomes 7. The material precipitate is eventually place in the oven at 70 °C for 60 minutes for producing a stable phase of nanoferrite powder.

## 2-3 PPy-NFs/Zn<sub>0.8</sub>Mn<sub>0.2</sub>Fe<sub>2</sub>O<sub>4</sub> preparation

We dissolved 0.03g of Zn<sub>0.8</sub>Mn<sub>0.2</sub>Fe<sub>2</sub>O<sub>4</sub> in 30 ml of distilled water and sonicated for ten hours and 0.03g of NFs PPy was dissolved in 30 ml of distilled water was sonicated for two hours. Then, Zn<sub>0.8</sub>Mn<sub>0.2</sub>Fe<sub>2</sub>O<sub>4</sub> solution had added to PPy-NFs solution in volumetric proportions. The resulting solution had sonicated for ten hour to get a homogeneous dispersion.

## 2-4 Thin film Preparation

We had utilized for photodetector application, n-type silicon (1×1) cm<sup>2</sup> substrate. The solutions of (PPy-NFs), (Zn<sub>0.8</sub>Mn<sub>0.2</sub>Fe<sub>2</sub>O<sub>4</sub>) and PPy-NFs nanocomposites were deposited on substrate by a drop-casting technique. The mask had made from Aluminum metal and then cast with pure and doped thin films as electrodes for light detector test.

## 3-Results and Discussion

### 3-1 X-ray diffraction measurements

X-ray diffractometer (XRD-6000, Shimadzu corporation, which is made Japan) operates at (40 kV and 30 mA) with Cu K (=1.5406), scan range: (10°-80°) had used to study the crystal structure to characterize the phase content of PPy-NFs and ferrite samples.

Figure 1 shows XRD patterns of PPy-NFs. X-ray diffraction studies show that the PPy-NFs powder is amorphous in nature that is non-crystalline solid where the distribution of atoms does not follow any crystalline system. The wide peak had resulted from dissipating X-rays from the chain of the PPy-NFs. In Fig. 1 broad peak was spotted at about 2θ = 24.5° which are assigned to the (102) directions(Sanches et al., 2015). The broad peak is a feature of amorphous PPy. A broad halo pattern at ranges 2θ = 10° - 35° is related to PPy-NFs that structured by the oxidative polymerization method and it is typical for doped structure of polypyrrole(MA, SG, PR, Shashwati, & VB, 2011; Ong, Ray, Cooney, Edmonds, & Easteal, 2008) [17,18]. According to the equation (1) that calculated the average chain separation (S) which calculates to be 4.53Å for polypyrrole nanofibers.

$$S = \frac{5\lambda}{8\sin\theta} \quad (1)$$

Here, λ and θ stands for the X-ray wavelengths and the diffraction angles at peaks of the amorphous Halo(Ceah, Forsyth, & Truong, 1998; Ouyang & Li, 1997) respectively.

As for the compound (Zn<sub>0.8</sub> Mn<sub>0.2</sub>Fe<sub>2</sub>O<sub>4</sub>) in Figure 2, The X-ray diffractometer had recorded for 2θ values ranging 10-80 degrees. A cell parameters are examined for XRD analysis where the major peaks are (111), (220), (311), (222), (400), (422), (511), (440) and (533). They had indexed well by using JCPDS # (74-2402), ICSD (01-074-2399) and Mn<sub>3</sub>O<sub>4</sub> card No.(024-0734). The ferrite sample reveal usual cubic spinel peaks (Space group: Fd3m) and a single-phase structure for (Zn<sub>0.8</sub>Mn<sub>0.2</sub>Fe<sub>2</sub>O<sub>4</sub>). As well It can conclude that Mn<sup>2+</sup>and Zn<sup>2+</sup> ions are replaced in the ferrite construction. Yet, the stage examination proved the existence of Mn<sub>3</sub>O<sub>4</sub> in the compositions and the width of peaks confirms nanosize particles.

The average crystallite size D<sub>ave</sub> had calculated by the following popular Scherrer expression:

$$D_{ave} = K\lambda/\beta \cos \theta \quad (2)$$

Here, K is the Scherrer constant and equal 0.94, λ is the wavelength of X-ray used, β refers to the full, at half maximum, width and θ is the Bragg angle. Volume of unit cell of the cubic structure by using equation (3) and The X-ray density d<sub>x</sub> were calculated from XRD data by using equation (4).

$$V_c = a_{exp}^3 \quad (3)$$

$$d_x = \frac{ZM}{N_A V_c} \quad (4)$$

Where Z and M are the formula units in unit cells (Z = 8 for spinel system) and the molecular weight of the samples respectively, N<sub>A</sub> is the number of Avogadro and V<sub>c</sub> refers to the volume of the cell (Syue, Wei, Chou, & Fu, 2011).

The zinc ferrite (Zn<sub>0.8</sub>Mn<sub>0.2</sub>Fe<sub>2</sub>O<sub>4</sub>) possesses normal spinel structures and Zn<sup>2+</sup> ions prefer the occupation of the tetrahedral site. The magnetic moments were seen in zinc ferrite with paramagnetic value (Standley, 1972). The zinc ions preferentially occupy the A-sites, whereas the Fe<sup>3+</sup> and Mn<sup>2+</sup> ions have an affinity for the A- and B-sites. The preparation technique and annealing temperature have a significant impact on the distribution of cation and structural characteristics (Kumar, Kumar, Narayan, & Kar, 2013). Mn<sub>1-x</sub>Zn<sub>x</sub>Fe<sub>2</sub>O<sub>4</sub> cation distribution expressed as: (Zn<sub>x</sub>Mn<sub>0.8-x</sub>Fe<sub>0.2</sub>)<sub>A</sub>[Mn<sub>0.2</sub>Fe<sub>1.8</sub>]<sub>B</sub>O<sub>4</sub><sup>2-</sup>, where an assign the tetrahedral and B assign the octahedral sites. The average cation radius at the tetrahedral and octahedral sites, r<sub>A</sub> and r<sub>B</sub> is measurable according to the cations distribution:

$$r_A = c(\text{Zn}_A^{2+}) \cdot r(\text{Zn}_A^{2+}) + c(\text{Mn}_A^{2+}) \cdot r(\text{Mn}_A^{2+}) + c(\text{Fe}_A^{3+}) \cdot r(\text{Fe}_A^{3+}) \quad (5a)$$

$$r_B = [c(\text{Mn}_B^{2+}) \cdot r(\text{Mn}_B^{2+}) + c(\text{Fe}_B^{3+}) \cdot r(\text{Fe}_B^{3+})] / 2 \quad (5b)$$

Here, c is the ionic concentrations at the tetrahedral and octahedral sites, r(Zn<sub>A</sub><sup>2+</sup>), r(Fe<sub>A</sub><sup>3+</sup>), r(Mn<sub>A</sub><sup>2+</sup>) which are the ionic radii of (0.60 Å), (0.49 Å) and (0.66 Å) ions in the tetrahedral sites respectively, r(Zn<sub>B</sub><sup>2+</sup>), r(Fe<sub>B</sub><sup>3+</sup>), r(Mn<sub>B</sub><sup>2+</sup>) which are the ionic radii of (0.74 Å), (0.645 Å) and (0.83 Å) ions in the octahedral sites, respectively were taken from Shannon (1976).

The theoretical lattice constant (a<sub>th</sub>) for Zn<sub>0.8</sub>Mn<sub>0.2</sub>Fe<sub>2</sub>O<sub>4</sub> system, on the basis of the estimated cation distribution, can be calculated by the relation:

$$a_{th} = \frac{8}{3\sqrt{3}} [(r_A + R_0) + (\sqrt{3}(r_B + R_0))] \quad (6)$$

Where R<sub>0</sub>: ionic radius of oxygen ion O<sup>2-</sup> (1.38 Å) (Tatarchuk, Bououdina, Paliychuk, Yaremiy, & Moklyak, 2017).

Tetrahedral bond lengths (d(MA-O)) are the distance between a tetrahedral cation and an anion, whereas octahedral bond lengths (d(MB-O)) are the distance between octahedral cations and anions, had given through the use of the relations (Cullity & Graham, 2011):

$$d(\text{MA} - \text{O}) = a\sqrt{3} (u - 0.25) \quad (7a)$$

$$d(\text{MB} - \text{O}) = a \sqrt{[3u^2 - 2.75u + \frac{43}{64}]} \quad (7b)$$

The distance between oxygen ions and cube faces is known as the oxygen positional parameter (u). For O atoms optimal close-packed arrangement, the ideal FCC parameters are (u = 0.375 = 3/8). The anion parameter (u) had determined by the following formula:

$$u = \left( \frac{r_A + R_0}{\sqrt{3} \cdot a_{exp}} \right) + 0.25 \quad (8)$$

To unit-cell origins at A-site, in which r<sub>A</sub> = A-site ionic radii, R<sub>0</sub> = 0.138 (nm), and a<sub>exp</sub> are the experimental lattice parameter (Satalkar & Kane, 2016). Based on the theoretical value of r<sub>A</sub>, an expected oxygen positioning parameter (u) had determined.

The packing of the ions in the ideal spinel structure seems ideal if the oxygen position parameter is (u = 3/8). Yet, anions in spinel ferrite usually deviate from their perfect positions by "δ" measured by formula (δ = u - 3/8).

The hopping lengths L<sub>A-A</sub>, L<sub>B-B</sub> and L<sub>A-B</sub> between the magnetic ion at the A-site and B-site obtained through (Naseri & Saion, 2012):

$$L_{A-A} = (a_{exp}\sqrt{3})/4 \quad (9a)$$

$$L_{B-B} = (a_{exp}\sqrt{2})/4 \quad (9b)$$

$$L_{A-B} = (a_{exp}\sqrt{11})/8 \quad (9c)$$

Where L<sub>B-B</sub>, L<sub>A-A</sub>, and L<sub>A-B</sub> are distances Octa-octa B-B, Tetra-tetra A-A, and Tetra-octa A-B, respectively.

Lattice constant (Å), average crystallite size, X-ray density, bonds lengths (Å), oxygen parameters, and hopping lengths for Zn<sub>0.8</sub>Mn<sub>0.2</sub>Fe<sub>2</sub>O<sub>4</sub> ferrite are presented in Table 1.

Table 1: XRD parameters of Zn<sub>x</sub>Mn<sub>1-x</sub>Fe<sub>2</sub>O<sub>4</sub> nanoparticles.

(x)	Lattice constant (Å)		Density of X-ray	crystallite size	Parameters of Oxygen		Length of Bond (Å)		Hopping length (Å)		
	a <sub>th</sub>	a <sub>exp</sub>	d <sub>x</sub> ( $\frac{g}{cm^3}$ )	D <sub>311</sub> (nm)	u	δ	d <sub>A-O</sub>	d <sub>B-O</sub>	L <sub>A-A</sub>	L <sub>B-B</sub>	L <sub>A-B</sub>
0.8	8.46	8.38	5.393	8.54	0.3867	0.0117	1.984	2.001	3.628	2.962	3.474

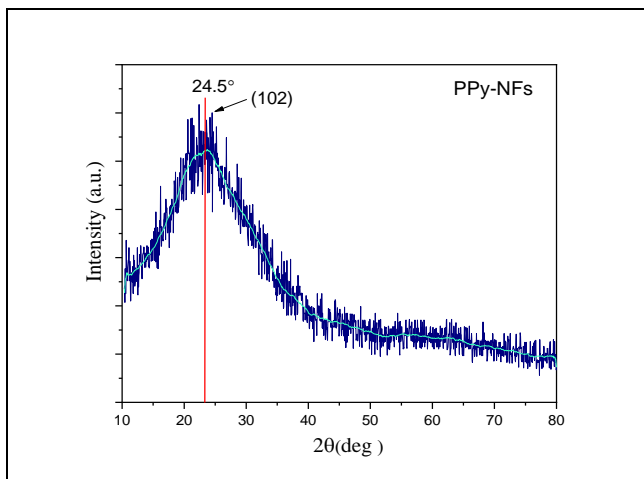


Figure 1: XRD pattern of (PPy-NFs).

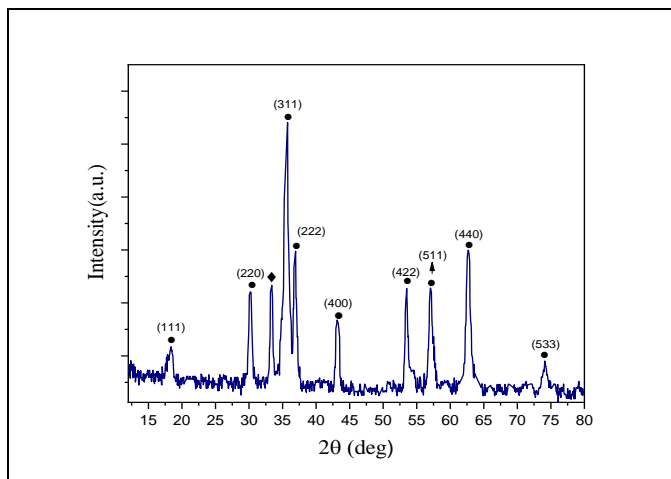


Figure 2: XRD result of Zn<sub>0.8</sub>Mn<sub>0.2</sub>Fe<sub>2</sub>O<sub>4</sub> nanoparticles.

### 3-2 FESEM image analysis

FE-SEM reveals topographical and morphological properties of the composites and pure materials. FESEM images of (PPy-NFs) samples synthesized by using the oxidative polymerization process are shown in Figure 3. It is observed that all the sample present (1-D) nanofibers, the nanofibers appear having rough surface and vary diameters, with tens of microns in length and diameter between  $\approx$  (50 and 130) nm. The micrograph clearly shows a typical FESEM image of doped PPy-NFs, as well as the fact that nanostructures are made up of a network of densely entangled twisted and coarse nanofibers.

FESEM image in Figure 4 for ferrite nanoparticles showing a denser view of the powder sample and homogeneous of grains distribution mostly. Also, the magnetic particles were closely packed and harmonic in the arrangement. These micrographs show nearly spherical particles with the size distributed in a range of  $\approx$  (13-20) nm. As a result, the surface morphological and microstructure images show good agreement with the XRD results. Only a few pores were found among the particles in the samples. Because of their magnetic characteristics, the magnetic nanoparticles tended to agglomeration together. Furthermore, particles agglomeration together due to emerging forces such as capillary, electrostatic, and Van-der-Wall forces, which cause mutual contacts between nanoparticles.

The decoration of Polypyrrole nanofibers/nanoferrite (PPy-NFs/ Zn<sub>0.8</sub>Mn<sub>0.2</sub>Fe<sub>2</sub>O<sub>4</sub>) had fabricated like a grainy surface structure. It had detected by FE-SEM. From Figure 5 the FE-SEM images show that the samples contain both nanoferrites stacked on the PPy-nanofibers surface. Therefore, Figure 5 reveals a gradual rise in ferrite on polymer fibers and enhancement in the attachment of ferrite particles. The magnetic particles are distributed uniformly on the conductive polymer matrix. This indicated that the composites had successfully mixed and blended homogeneously. The ferrite concentration seems useful in occupation the polymer porous sites, increase the interaction surface area and Surface energy. All of these lead to improvement of various structural and electrical properties. Thus, a change would occur in the physical properties such as the shape, size, appearance and state of the material without affecting the internal structure. As, the fibers roughness greatly influence the adhesion strength between the particle and the fiber. Histograms represent diameters distribution of PPy-NFs and Zn<sub>0.8</sub>Mn<sub>0.2</sub>Fe<sub>2</sub>O<sub>4</sub> nanoparticles that calculated by Image J software. It confirmed a well agreement with FE-SEM test that shown in Figure 6.

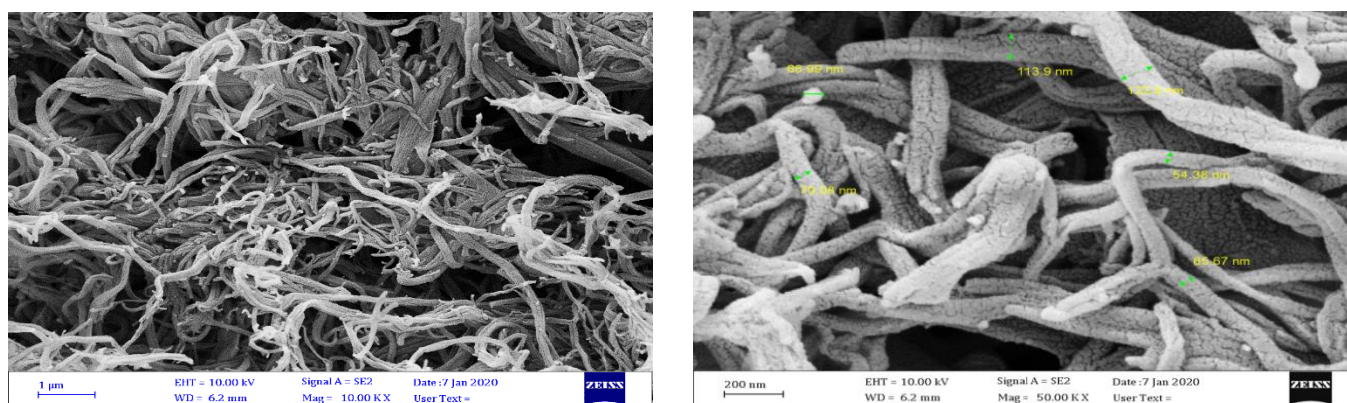


Figure 3: FE-SEM images of PPy-NFs at different magnification.

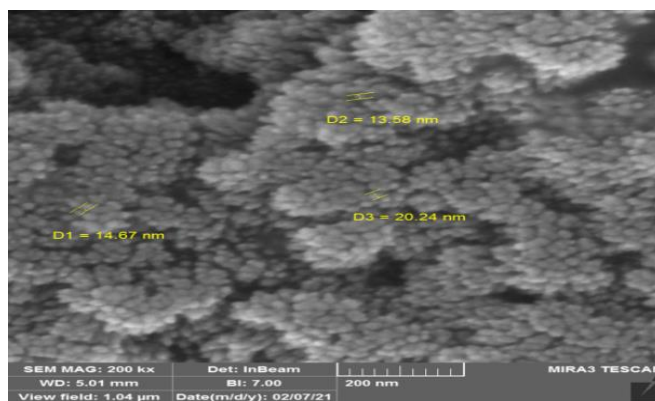
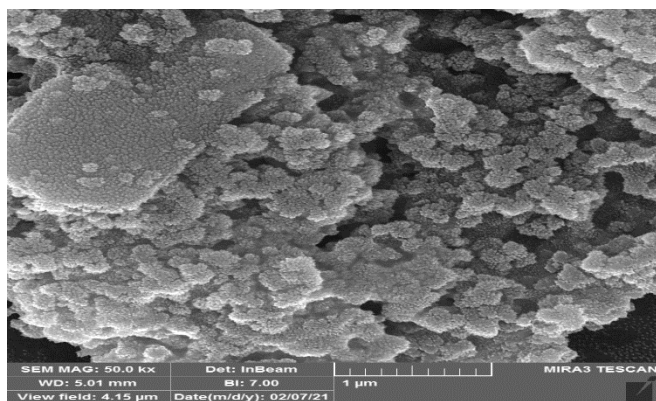


Figure 4: FE-SEM images of  $Zn_{0.8}Mn_{0.2}Fe_2O_4$  nanoparticles at different magnification.

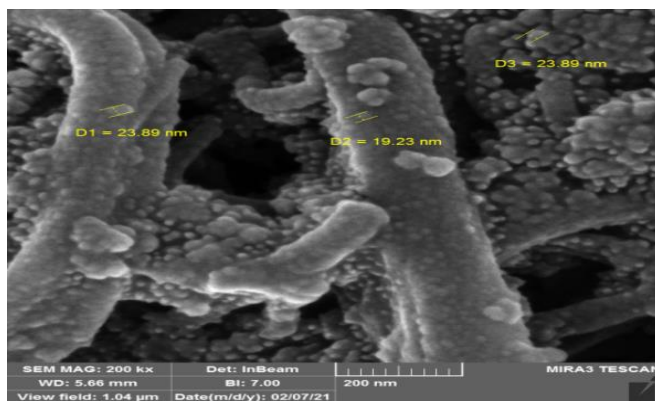
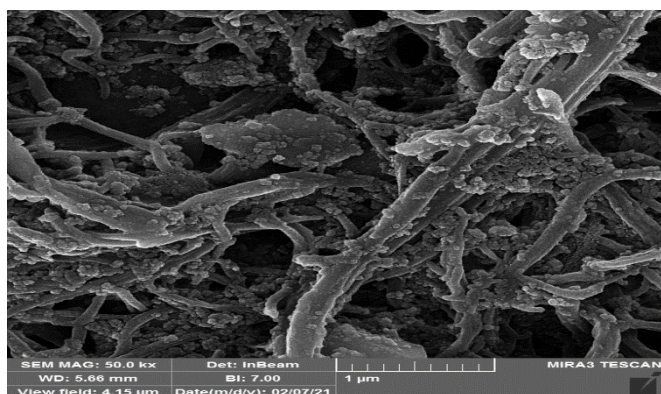


Figure 5: FE-SEM images of (PPy-NFs/ $Zn_{0.8}Mn_{0.2}Fe_2O_4$ ) nanocomposite at different magnification.

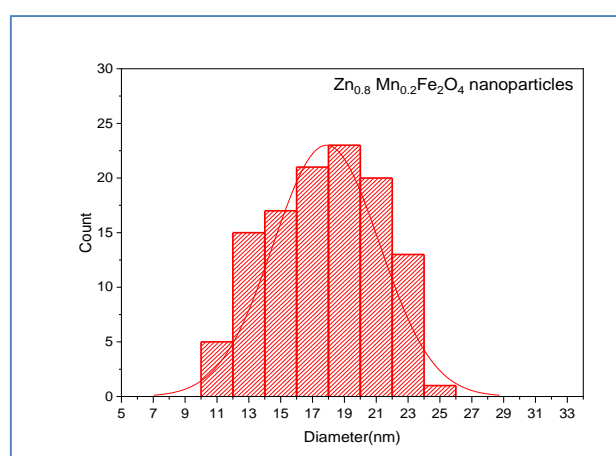
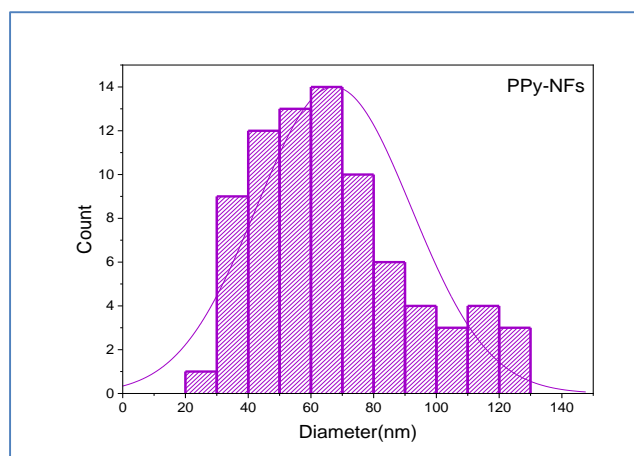


Figure 6: Histograms showing the diameter distribution of PPy-NFs and  $Zn_{0.8}Mn_{0.2}Fe_2O_4$  nanoparticles.

### 3-3 Optical properties

Optical spectroscopy is an important tool for understanding the behavior of nanocomposites and the conducting states corresponding to the absorption bands of inter and intra gap states of conducting polymers (CPs). Figure 7 represents the absorbance spectra of PPy-NFs that recorded over the range (200-1100) nm by using Shimadzu UV-1800 UV-Visible Scanning Spectrophotometer.

PPy-NFs spectrum reveals peak at 315 nm and broad absorption bands ranging 450-550 nm. The former peak added to the  $\pi - \pi^*$  inter band transitions. In particular, the move to the conduction bands of neutral states of PPy-NFs from valence bands (Wang, Zhao, & Yu, 2015). As the broad absorption band shows polymerization (Konwer, Maiti, & Dolui, 2011). It may be assigned to polaron band transitions which correspond with (Chen et al., 2015).

The significant absorption at  $\approx 600$  nm denoting the free carrier tail of oxidized polypyrrole. The absorption peak shifts with the number of available delocalized electrons, depending on the chain length. This UV-Vis spectrum gives confirmation to formed material as polypyrrole. The ratio of the two absorbance maxima reflect the doping level of the polymer which itself depend on the oxidation degree and the conjugation length (Kepas, Grzeszczuk, Kvarnstrom, Lindfors, & Ivaska, 2007). Figure 8 represents the plot between  $(\alpha h\nu)^2$  and  $h\nu$  for PPy-NFs samples. It was observed that the optical energy band gap of PPy-NFs sample is about (3.90) eV. This value is close to what Hasan, Bakr, and Ibrahim (2021).

UV-Vis spectra for ferrite sample is recorded in the range 200-1100 nm. Figure 8 represents the plot between  $(\alpha h\nu)^2$  and  $h\nu$  for  $Zn_{0.8}Mn_{0.2}Fe_2O_4$  sample. The optical energy bandgap value is about (3.80 eV).

The UV-Vis absorption spectra of the PPy-NFs/  $Zn_{0.8}Mn_{0.2}Fe_2O_4$  nanocomposites had showed in Figure 7. The ultraviolet-visible absorption spectra for polypyrrole nanofibers/ $Zn_{0.8}Mn_{0.2}Fe_2O_4$  show two absorption bands at (300, 345) and (455,545) nm. In wavelength band (300, 345) nm, the peak is given to the  $\pi-\pi^*$  movement of the benzenoid ring. The other peak in wavelength absorption band (455, 545) nm is attributed to polaron- $\pi^*$  transitions(Mehto, Mehto, Chauhan, Singh, & Pandey, 2017).

The location of the observed absorption peak in PPy-NFs/  $Zn_{0.8}Mn_{0.2}Fe_2O_4$  nanocomposite had changed in comparison with PPy-NFs positions. The interaction between magnetic nanoparticles (MNs) and polypyrrole nanofibers could explain the observed shift in the typical peak positions(Mahto, Chowdhuri, & Sahu, 2014). Figure 8 represent the plot between  $(\alpha h\nu)^2$  and  $h\nu$  for PPy-NFs/  $Zn_{0.8}Mn_{0.2}Fe_2O_4$  samples. Where the optical energy bandgap value is about (4.95 eV).

This optical band gap energy ( $E_g$ ) values are explained according to ions distributions at lattice sites of ferrite constructure. The zinc ions would prefer strongly tetrahedral [A] sites, yet iron cations and  $Mn^{2+}$  ions could be occupying the octahedral (B) and tetrahedral [A] sites(Ati, Othaman, & Samavati, 2013; Zare, Ati, Dabagh, Rosnan, & Othaman, 2015). The electronic conduction mechanism in unit cell of spinel ferrite primarily emerge from the jumping of electrons between ferrous ( $Fe^{2+}$ )/ferric ( $Fe^{3+}$ ) ions at B symmetry sites(Qindeel & Alonizan, 2018). The  $Mn^{2+}$  and  $Zn^{2+}$  are oxidized to  $Mn^{3+}$  and  $Zn^{3+}$  when deposition processes and provide a positive hole, gives specific values for the energy gap(Ashiq, Naz, Malana, Gohar, & Ahmad, 2012).

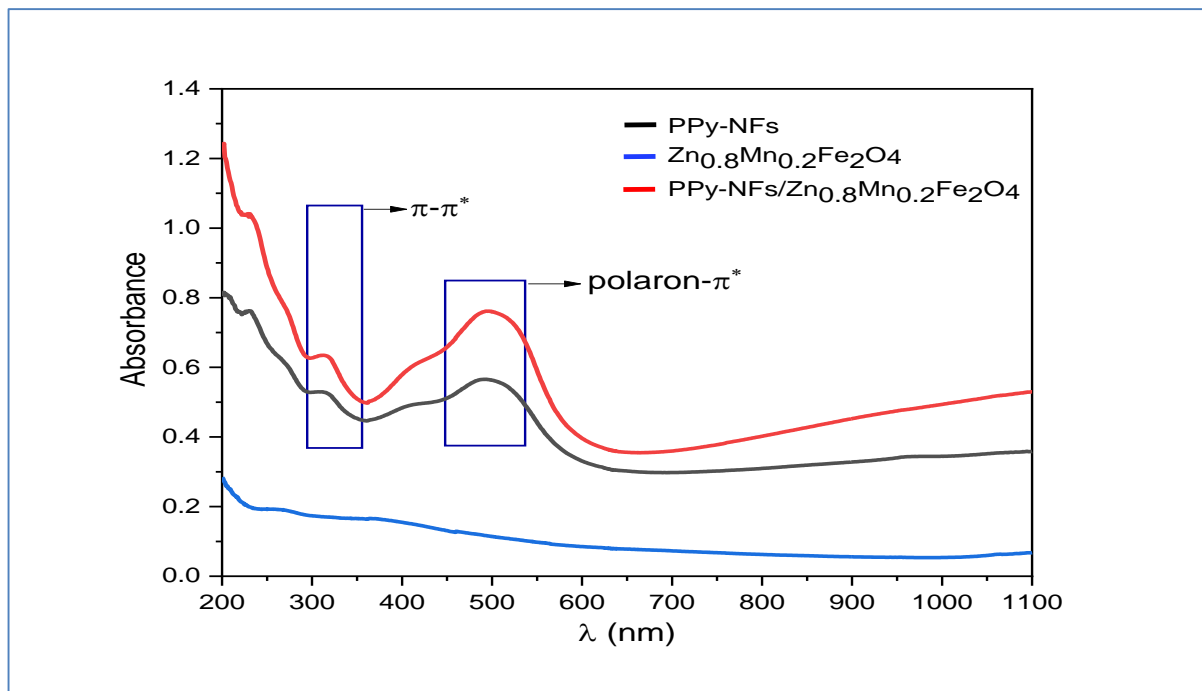
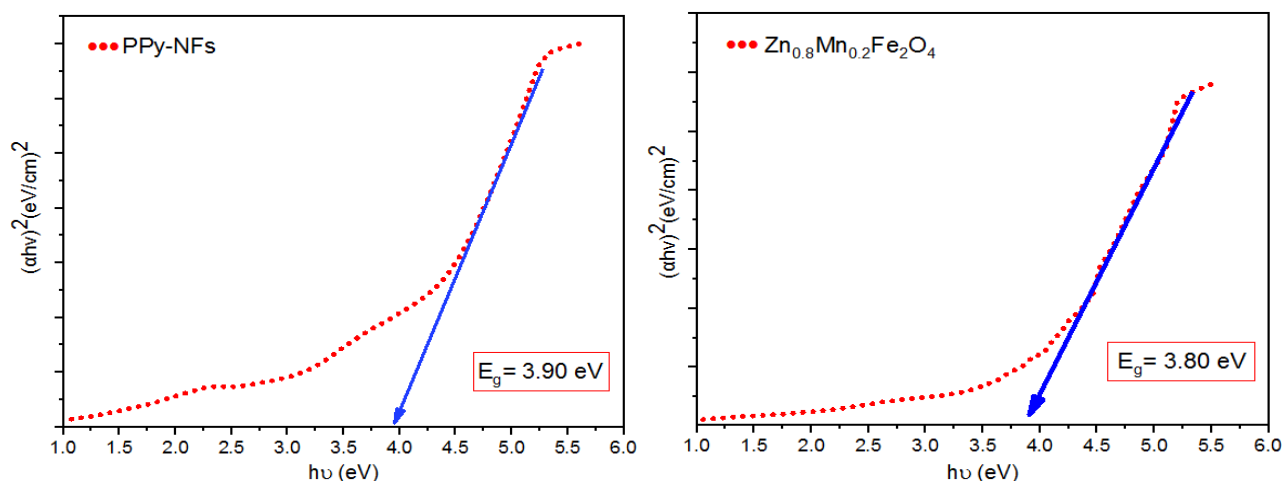


Figure 7: Absorption spectra for PPy-NFs,  $Zn_{0.8}Mn_{0.2}Fe_2O_4$  and PPy-NFs/ $Zn_{0.8}Mn_{0.2}Fe_2O_4$ .



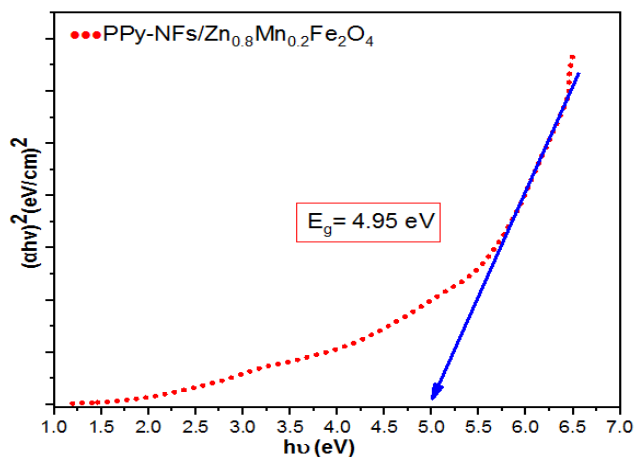


Figure 8: Estimation of optical band gap energy of PPy-NFs,  $Zn_{0.8}Mn_{0.2}Fe_2O_4$  and PPy-NFs/ $Zn_{0.8}Mn_{0.2}Fe_2O_4$ .

### 3-4 The photosensitivity

The studies of pristine and doped samples had carried out with light and without light. The photocurrent response versus time differences for various samples. The following equation is used to find the photoconductor detector's sensitivity value.

$$S (\%) = \frac{I_{\text{light}} - I_{\text{dark}}}{I_{\text{dark}}} \times 100 \quad (10)$$

Where  $I_{\text{light}}$  represents light current, and  $I_{\text{dark}}$  represents the dark current.

The conductivity rises when the light is switched on, and if the light is switched off, the current goes back to its normal rates. As shown in the diagrams below, this action is repeated numerous times, with the rise and fall times for each condition being equal to (0.5) seconds (on, off). For photoexcitation-induced current in samples, current time features (I-t) were measured at wavelengths (405) nm and varied light powers (10 mW, 15 mW, 20 mW, and 30 mW).

Figure 9 shows the slight photocurrent reaction of polypyrrole nanofibers had attributed to many reasons firstly the low light absorption and the limitation of penetration depth for incident photons, secondly, in case of high rate of recombination of photogenerated charges(Liu et al., 2016) and thirdly maybe to the structural disorder pattern in pure PPy sample as evident from XRD and FE-SEM results(Singh & Shukla, 2015).

In the  $Zn_{0.8}Mn_{0.2}Fe_2O_4$  sample, it is necessarily to mention some observation was given to photodetectors that is based ferrite. Yet, they often show good optical absorptions in the visible regions. The photocurrents of the Nanoferrite are moderate in compared with other ferrites. However, the photocurrent intensity is influences significantly by numerous check circumstances such as apparatus configuration, light intensity and wavelength as well as external applied bias(Zhai et al., 2009; Zhai et al., 2011).

Figure 10 displays the measured photocurrents versus the time of the Nanoferrite samples under illumination from the 405 nm laser with different energy powers at room temperature. The photocurrents seem to rapidly reach a stable state after turning on a 504 nm laser. It is then quickly reduced when the laser is off.

Table 3 shows the photocurrents VS the laser powers (10 mW, 15 mW, 20 mW and 30 mW), in addition increase and decrease of photocurrent time generated.

There is a positive linear relation between the amounts of the photocurrent with incident laser power from 10 mW to 30 mW.

In order to improve low photosensitivity of polypyrrole, several strategies have been followed, such as decoration of conductive polymers molecules by nanoferrite materials to extend and enhance the photon adsorption, as well as the fabrication of harmonious structures to promote wavelength selectivity and charge transport. There is a clear improvement in the sensitivity rate through PPy-NFs that doping by  $Zn_{0.8}Mn_{0.2}Fe_2O_4$  which exhibit in the Figure11. However, The PPy with nanoferrite clearly showed an increased photocurrent response in compared with PPy because of the absorbed photons of polypyrrole (PPy-NFs) that caused the electron movement from the HOMO (biggest employed molecular orbital) to the (LUMO) (smallest unoccupied molecular orbital) in laser 405 nm. So the number of free electrons and electron-holes pairs increases and raise electrical conductivity and low dark current values.

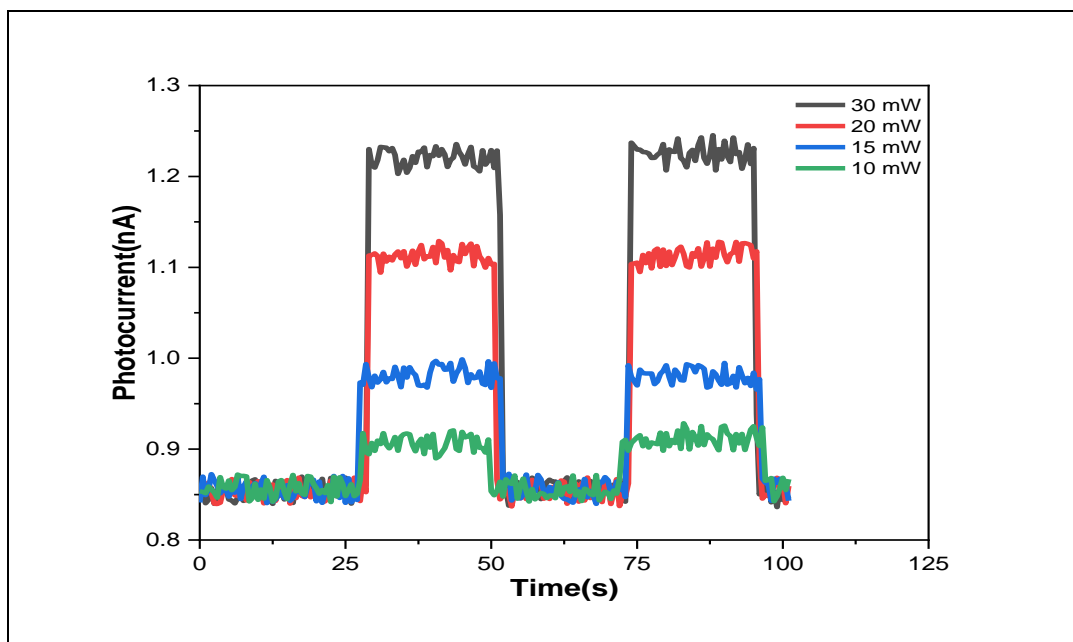


Figure 9: Variation of light sensitivity for PPy-NFs with various energy powers.

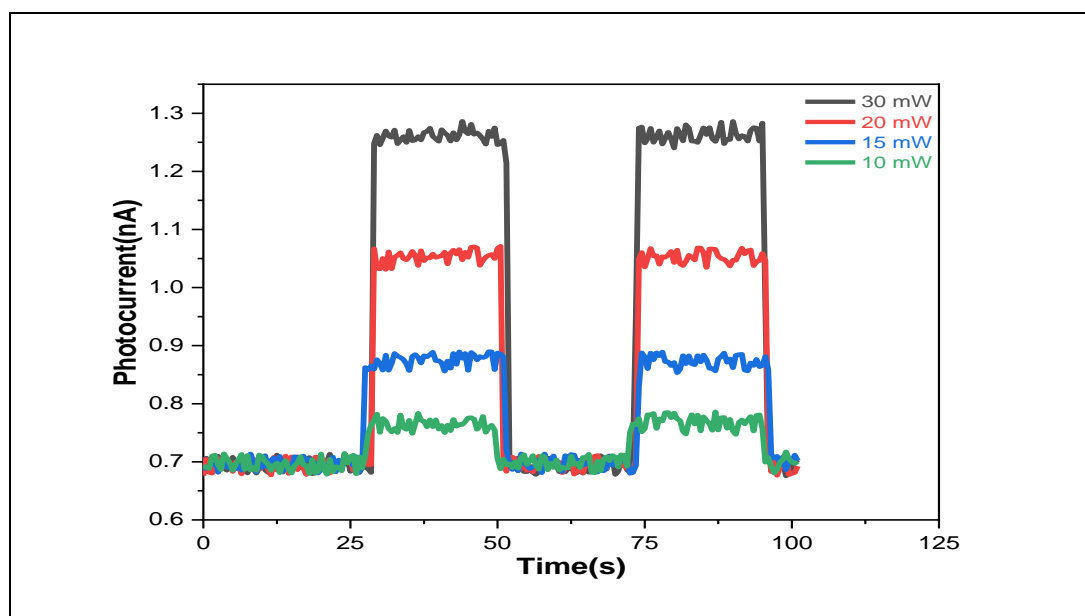


Figure 10: Variation of light sensitivity for  $Zn_{0.8}Mn_{0.2}Fe_2O_4$  with various energy powers.

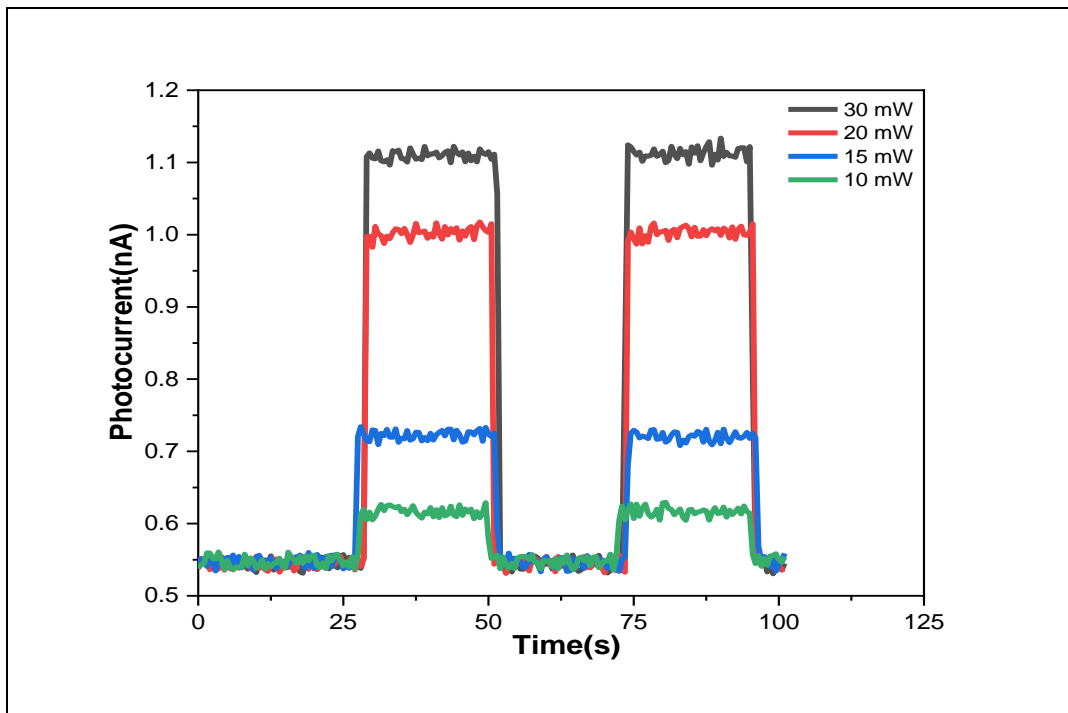


Figure 11: Variation of light sensitivity for PPy-NFs/ $Zn_{0.8}Mn_{0.2}Fe_2O_4$  with various energy powers.

Table 2: Sensitivity variation of prepared materials.

sample	Sensitivity (30 mW)	Sensitivity (20 mW)	Sensitivity (15 mW)	Sensitivity (10 mW)	Rise Time(s)	Fall Time(s)
PPy-NFs	43.42 %	31.10 %	14.78 %	7.15 %	$5 \times 10^{-1}$	$5 \times 10^{-1}$
$Zn_{0.8}Mn_{0.2}Fe_2O_4$	81.47 %	66.99 %	35.01 %	16.75 %	$5 \times 10^{-1}$	$5 \times 10^{-1}$
PPy-NFs / $Zn_{0.8}Mn_{0.2}Fe_2O_4$	103.74 %	84.27 %	36.8 %	17.25 %	$5 \times 10^{-1}$	$5 \times 10^{-1}$

#### 4- Conclusions

Polypyrrole nanofibers with several diameters were synthesized successfully by chemical polymerization technique. As well as, Nanoparticles of  $Zn_{0.8}Mn_{0.2}Fe_2O_4$  were performed by the co-precipitation technology, combined with the hydrothermal synthesis. The composite film of PPy and magnetic nanoparticles is a good electrode material for light detectors. The maximum sensitivity values of the photosensors were obtained from PPy nanofibers doped with nanoferrite for wavelength 405nm. Important improvements in light sensitivity and on / off ratio are observed when the conducting polymer (PPy-NFS) was decorated with ferrite particles, thus doping insertions can rise the sensitivity of the polypyrrole nanofibers photodetector.

#### References

- Ashiq, M. N., Naz, F., Malana, M. A., Gohar, R. S., & Ahmad, Z. (2012). Role of Co–Cr substitution on the structural, electrical and magnetic properties of nickel nano-ferrites synthesized by the chemical co-precipitation method. *Materials Research Bulletin*, 47(3), 683-686.
- Ati, A. A., Othaman, Z., & Samavati, A. (2013). Influence of cobalt on structural and magnetic properties of nickel ferrite nanoparticles. *Journal of Molecular Structure*, 1052, 177-182.
- Caruso, F. (2001). Nanoengineering of particle surfaces. *Advanced materials*, 13(1), 11-22.
- Cheah, K., Forsyth, M., & Truong, V.-T. (1998). Ordering and stability in conducting polypyrrole. *Synthetic metals*, 94(2), 215-219.

- Chen, X., Yu, N., Zhang, L., Liu, Z., Wang, Z., & Chen, Z. (2015). Synthesis of polypyrrole nanoparticles for constructing full-polymer UV/NIR-shielding film. *RSC advances*, 5(117), 96888-96895.
- Cullity, B. D., & Graham, C. D. (2011). *Introduction to magnetic materials*: John Wiley & Sons.
- Ding, H., Liu, X.-M., Wan, M., & Fu, S.-Y. (2008). Electromagnetic functionalized cage-like polyaniline composite nanostructures. *The Journal of Physical Chemistry B*, 112(31), 9289-9294.
- Ding, S.-J., Zhang, C.-L., Yang, M., Qu, X.-Z., Lu, Y.-F., & Yang, Z.-Z. (2006). Template synthesis of composite hollow spheres using sulfonated polystyrene hollow spheres. *Polymer*, 47(25), 8360-8366.
- Feng, X., Mao, C., Yang, G., Hou, W., & Zhu, J.-J. (2006). Polyaniline/Au composite hollow spheres: synthesis, characterization, and application to the detection of dopamine. *Langmuir*, 22(9), 4384-4389.
- Hasan, M. I., Bakr, N. A., & Ibrahim, I. M. (2021). Morphological, magnetic, optical, surface potential, and H<sub>2</sub>S gas sensing behavior of polypyrrole nanofibers. *Journal of Electronic Materials*, 50(5), 2716-2724.
- Jiang, J., Li, L. C., & Xu, F. (2006). Preparation, characterization and magnetic properties of PANI/La-substituted LiNi ferrite nanocomposites. *Chinese Journal of Chemistry*, 24(12), 1804-1809.
- Kepas, A., Grzeszczuk, M., Kvarnstrom, C., Lindfors, T., & Ivaska, A. (2007). UV-Vis and Raman spectroelectrochemistry of electrodeposited polypyrrole in hexafluorophosphate. *Polish Journal of Chemistry*, 81(12), 2207.
- Konwer, S., Maiti, J., & Dolui, S. K. (2011). Preparation and optical/electrical/electrochemical properties of expanded graphite-filled polypyrrole nanocomposite. *Materials Chemistry and Physics*, 128(1-2), 283-290.
- Kumar, L., Kumar, P., Narayan, A., & Kar, M. (2013). Rietveld analysis of XRD patterns of different sizes of nanocrystalline cobalt ferrite. *International Nano Letters*, 3(1), 1-12.
- Li, L., Jiang, J., & Xu, F. (2006). Novel polyaniline-LiNiO. 5La<sub>0</sub>. 02Fe<sub>1</sub>. 98O<sub>4</sub> nanocomposites prepared via an in situ polymerization. *European polymer journal*, 42(10), 2221-2227.
- Liu, Y., Ma, H., Zhang, Y., Pang, X., Fan, D., Wu, D., & Wei, Q. (2016). Visible light photoelectrochemical aptasensor for adenosine detection based on CdS/PPy/g-C<sub>3</sub>N<sub>4</sub> nanocomposites. *Biosensors and Bioelectronics*, 86, 439-445.
- Lu, X., Yu, Y., Chen, L., Mao, H., Gao, H., Wang, J., . . . Wei, Y. (2005). Aniline dimer-COOH assisted preparation of well-dispersed polyaniline-Fe<sub>3</sub>O<sub>4</sub> nanoparticles. *Nanotechnology*, 16(9), 1660.
- MA, C., SG, P., PR, G., Shashwati, S., & VB, P. (2011). Synthesis and characterization of polypyrrole (PPy) thin films. *Soft nanoscience letters*, 2011.
- Mahto, T. K., Chowdhuri, A. R., & Sahu, S. K. (2014). Polyaniline-functionalized magnetic nanoparticles for the removal of toxic dye from wastewater. *Journal of applied polymer science*, 131(19).
- Mehto, A., Mehto, V. R., Chauhan, J., Singh, I., & Pandey, R. (2017). Preparation and characterization of polyaniline/ZnO composite sensor. *J. Nanomed. Res*, 5, 00104.
- Nalwa, H. S. (2003). *Handbook of organic-inorganic hybrid materials and nanocomposites*: American Scientific Publishers.
- Naseri, M. G., & Saion, E. B. (2012). Crystalization in spinel ferrite nanoparticles. *Advances in crystallization processes*, 349-380.
- Niu, Z., Yang, Z., Hu, Z., Lu, Y., & Han, C. C. (2003). Polyaniline-silica composite conductive capsules and hollow spheres. *Advanced Functional Materials*, 13(12), 949-954.
- O'Hendley, R. (1999). Modern magnetic materials. *Principles and Applications (Johns Wiley & Sons, Inc., 2000)*.
- Ong, C. K., Ray, S., Cooney, R. P., Edmonds, N. R., & Easteal, A. J. (2008). Preparation and characterization of composites of polyethylene with polypyrrole-coated wollastonite. *Journal of applied polymer science*, 110(1), 632-640.
- Ouyang, J., & Li, Y. (1997). Great improvement of polypyrrole films prepared electrochemically from aqueous solutions by adding nonaphenol polyethyleneoxy (10) ether. *Polymer*, 38(15), 3997-3999.
- Qindeel, R., & Alonizan, N. H. (2018). Structural, dielectric and magnetic properties of cobalt based spinel ferrites. *Current Applied Physics*, 18(5), 519-525.
- Reddy, M. P., Zhou, X., Huang, Q., & Reddy, R. R. (2014). Synthesis and characterization of ultrafine and porous structure of magnesium ferrite nanospheres. *Int J Nano Stud Technol*, 3(6), 72-77.
- Sanches, E. A., Alves, S. F., Soares, J. C., da Silva, A. M., da Silva, C. G., de Souza, S. M., & da Frota, H. O. (2015). Nanostructured polypyrrole powder: a structural and morphological characterization. *Journal of Nanomaterials*, 2015.
- Satalkar, M., & Kane, S. (2016). *On the study of Structural properties and Cation distribution of Zn<sub>0</sub>. 75-xNi<sub>x</sub>Mg<sub>0</sub>. 15Cu<sub>0</sub>. 1Fe<sub>2</sub>O<sub>4</sub> nano ferrite: Effect of Ni addition*. Paper presented at the Journal of Physics: Conference Series.
- Shannon, R. D. (1976). Revised effective ionic radii and systematic studies of interatomic distances in halides and chalcogenides. *Acta crystallographica section A: crystal physics, diffraction, theoretical and general crystallography*, 32(5), 751-767.
- Singh, S. K., & Shukla, R. (2015). Optical and photoconductivity properties of pure Polypyrrole and titanium dioxide-doped Polypyrrole nanocomposites. *Materials Science in Semiconductor Processing*, 31, 245-250.

Standley, K. J. (1972). *Oxide magnetic materials*: Oxford University Press, USA.

Syue, M.-R., Wei, F.-J., Chou, C.-S., & Fu, C.-M. (2011). Magnetic, dielectric, and complex impedance properties of nanocrystalline Mn–Zn ferrites prepared by novel combustion method. *Thin Solid Films*, 519(23), 8303-8306.

Tatarchuk, T., Bououdina, M., Paliychuk, N., Yaremiy, I., & Moklyak, V. (2017). Structural characterization and antistructure modeling of cobalt-substituted zinc ferrites. *Journal of Alloys and Compounds*, 694, 777-791.

Velusamy, S., Ahamed, M., & Punniyamurthy, T. (2004). Novel polyaniline-supported molybdenum-catalyzed aerobic oxidation of alcohols to aldehydes and ketones. *Organic letters*, 6(26), 4821-4824.

Wang, A., Zhao, W., & Yu, W. (2015). Effect of acid/base on the third-order optical nonlinearity of polypyrrole. *Journal of Molecular Structure*, 1099, 291-296.

Xiao, Y., & Li, C. M. (2008). Nanocomposites: from fabrications to electrochemical bioapplications. *Electroanalysis: An International Journal Devoted to Fundamental and Practical Aspects of Electroanalysis*, 20(6), 648-662.

Zare, S., Ati, A. A., Dabagh, S., Rosnan, R., & Othaman, Z. (2015). Synthesis, structural and magnetic behavior studies of Zn–Al substituted cobalt ferrite nanoparticles. *Journal of Molecular Structure*, 1089, 25-31.

Zhai, T., Fang, X., Liao, M., Xu, X., Zeng, H., Yoshio, B., & Golberg, D. (2009). A comprehensive review of one-dimensional metal-oxide nanostructure photodetectors. *Sensors*, 9(8), 6504-6529.

Zhai, T., Li, L., Ma, Y., Liao, M., Wang, X., Fang, X., . . . Golberg, D. (2011). One-dimensional inorganic nanostructures: synthesis, field-emission and photodetection. *Chemical Society Reviews*, 40(5), 2986-3004.

Zhong-ai, H., Hong-xiao, Z., Chao, K., Yu-ying, Y., Xiu-li, S., Li-jun, R., & Yan-peng, W. (2006). The preparation and characterization of quadrate NiFe<sub>2</sub>O<sub>4</sub>/polyaniline nanocomposites. *Journal of Materials Science: Materials in Electronics*, 17(11), 859-863.